Design of a Smart 3D-printed Wristed Robotic Surgical Instrument with Embedded Force Sensing and Modularity

Carlo A. Seneci, Konrad Leibrandt, Piyamate Wisanuvej, Jianzhong Shang, Ara Darzi, Guang-Zhong Yang *Fellow, IEEE*

***Abstract* — This paper introduces the design and characterization of a robotic surgical instrument produced mainly with rapid prototyping techniques. Surgical robots have generally complex structures and have therefore an elevated cost. The proposed instrument was designed to incorporate minimal number of components to simplify the assembly process by leveraging the unique strength of rapid prototyping for producing complex, assemble-free components. The modularity, cost-effectiveness and fast manufacturing and assembly features offer the possibility of producing patient or task specific instruments. The proposed robot incorporates an integrated force measurement system, thus allowing the determination of the force exchanged between the instrument and the environment. Detailed experiments were performed to validate the functionality and force sensing capability of the instrument.**

I. Introduction

Rapid prototyping, also known as 3D printing or additive manufacturing, is increasingly popular as an alternative solution to traditional manufacturing technologies. It is cost-effective, especially for small batch productions. The cost-effectiveness is due to the elimination of tooling and setup time necessary in traditional manufacturing techniques, which is relatively high at low volume production. In addition, 3D printing has demonstrated that it can drastically reduce the time of design iterations, allowing designer to evaluate more extensively their creations. In recent years, academic and industrial research and development efforts on additive manufacturing have been fast accelerating, with the objective to study, understand and fully control the advantages of the processes of additive manufacturing [1]. On the other hand, since this is a relatively young technology, its use has not yet been fully integrated into the production chain. This calls for new production paradigms and allows additive manufacturing to complement with existing industrial processes. An example of this trend is the machine Lasertec 65 by Mori or the Lumex Avance-25 by Matsuura, which combine the strength of additive and subtractive manufacturing. Objects with complex structures are produced directly from additive manufacturing, and then surfaces with high surface and tolerance requirements are processed with subtractive manufacturing, hence achieve minimal material waste and high quality requirements. Present technology is also capable of printing multiple materials and also creating combinations of them. This represents a great opportunity for designers and engineers to create systems with embedded features that cannot be achieved otherwise. Many examples of the usage of rapid prototyping in different fields of application can be found in literature. For example, Ahn et al. used 3D printing to produce a smart soft composite capable of exploiting the different stiffness of the materials that compose it, to realize bending motions [2].

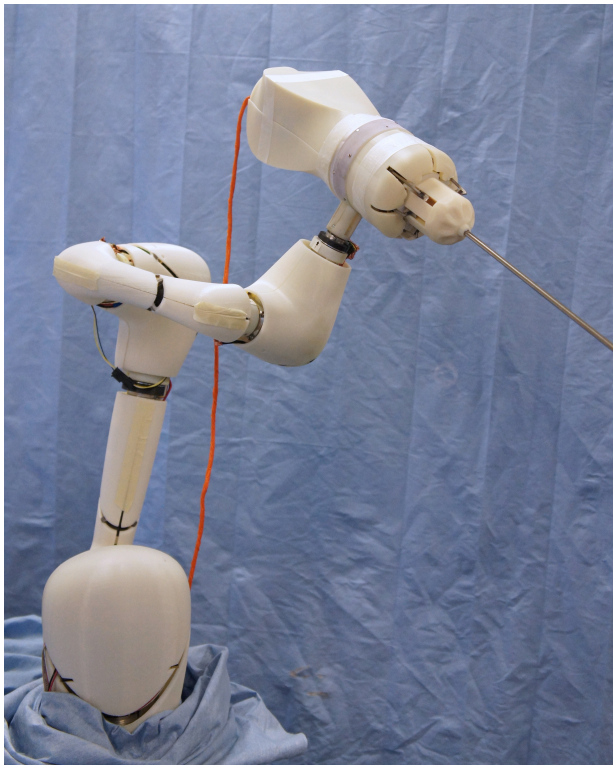

Figure 1. Wristed surgical robot mounted on a 6 DoF serial manipulator for global positioning.

In the medical field, rapid prototyping has found important roles, especially in the creation of patient specific implants, such as dental implants [3], where prosthetic teeth are produced as a copy of the original ones. In orthopedics, where prosthetic implants could now be specifically designed and produced for patients [4], similarly to the case of reconstructive surgery [5], rapid prototyping, has not only found its way in the manufacturing of implants; but also in the manufacturing of tooling and functioning devices. Some of these are parts of surgical robots, demonstrating the large applicability of this technology in the production chain. A snake-like surgical robot was produced using Selective Laser Sintering (SLS) of Nylon, producing the flexible backbone of the bi-manual continuum robot [6]. Its design and production could have only been achieved through the use of additive

Carlo A. Seneci, Konrad Leibrandt, Piyamate Wisanuvej, Jianzhong Shang, Ara Darzi and Guang-Zhong Yang are with the Hamlyn Centre for Robotic Surgery, Imperial College London. Email: c.seneci@imperial.ac.uk

manufacturing, given the complexity of the components. Another example originated from the surgical field is a Micro-Electro-Mechanical Systems (MEMS) for the removal of heart tissue, where the components were generated with lithography and pre-assembled components with moving parts were produced [7]. Rapid prototyping finds its integral deployment when considerations about its main principles and advantages are implemented during the design phase. At this stage, it is possible to design components that can be rapidly manufactured and assembled, leading the way to rapid manufacturing. The reduction of production time is one of the main results for this technology making it cost-competitive, when fully exploited. The authors' previous work was conducted to study the process of Selective Laser Melting (SLM), to produce fully dense functional components to be used to build a surgical robot and its instruments [8]. Concepts of rapid manufacturing and assembly were formulated to make full use of the flexibility of this technology.

This work presents the design and manufacturing of a surgical robot that mounts a wristed instrument that is rapidly manufactured and assembled. The robot has also been designed to allow quick integration of new instruments, giving importance to the modularity of the design. Finally, this robot has integrated force sensing into its actuation, in order to implement force feedback in a cost-effective way, by avoid placing force sensors on the surgical instrument tip, which is a major barrier of sensing integration in current surgical robotics.

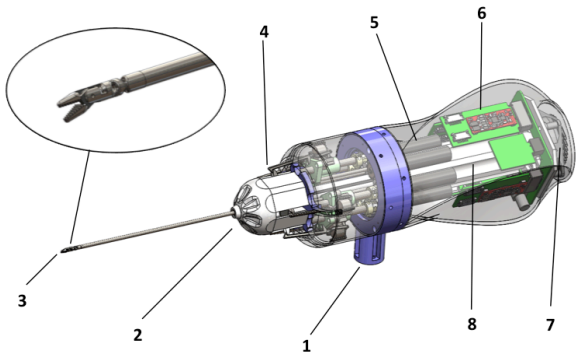

Figure 2. Overview of the surgical robot with mounted instrument: (1) interface with the serial arm, (2) surgical instrument, (3) wristed grasper, (4) fast couplings, (5) brushless motors, (6) driving electronics, (7) fan and (8) main body.

II. Overview and Design

A. Conceptual Design Overview

The surgical robot presented in this work was designed to be a modular attachment for the 6 DoF serial manipulator presented in Fig. 1. The idea is to use the serial manipulator to provide the robotic tool with global positioning and a Remote Centre of Motion (RCM), specifically with 2 perpendicular rotations and one translation. The surgeon is provided with 3 additional DoFs by the end-effector, 2 DoF wrist and axial rotation. The surgical robot provides an instrument's mounting interface with fast couplings to give the freedom to attach surgical tools. The wristed grasper presented here was designed to be disposable and to have a diameter of Ø3mm, which could be used for applications where the surgical site is characterized by narrow space. The advantage of embedded force sensing also allows the deployment of this robot in areas where the instrument-tissue interaction is very delicate, for example in brain or fetal surgery. The system uses three pairs of antagonistic tendons to drive the end-effector. Instead of using three motors to drive the three pairs of tendon, as in most tendon driven systems, this device uses six actuators to drive the six tendons, which makes it a redundant actuation. This combined with the use of a load cell on each tendon to monitor the tension of all tendons, allows for more precise instrument control while providing embedded force sensing. When an instrument is plugged onto the robot, the robot starts to pull back all the tendons until the set pretension of 2N is achieved on each tendon. At this stage the initial position has been identified and the robot can actuate the tendons, whilst maintaining the pretension and compensation for possible backlash.

B. Robot Mechanical Design

The proposed robot design consists of a cylindrical body which hosts all the main components of the robot, from motors and driving electronics to the actuation mechanisms and the fast couplings (Fig. 2). All the seven motors used for this robot are DC brushless Maxon EC 13 Ø13mm 12W, with planetary gearhead with reduction ratio of 67:1. The motor driving electronics is placed at the back of the motors, directly mounted on the main body of the instrument. The driving electronics contains the power circuitry and the communication one. The power provided to the robot is 24VDC and the communication used is a customized RS-485 protocol running at 4MBaud. The driving electronics is composed of a motherboard that allocates 8 slots for plugging in the motor controller boards and one for the voltage regulator board. The motherboard also hosts the connector for the multicore-shielded cable used to transfer power and communication between the robot and the host computer and power supply.

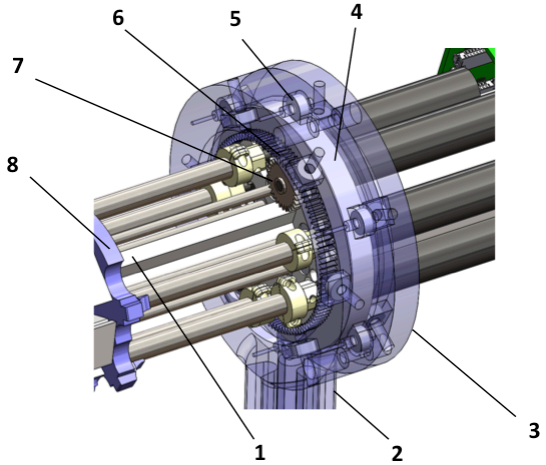

Figure 3. Detailed view of the main body rotation mechanism: (1) main body, (2) interface with the serial arm, (3) interface's back plate, (4) main body's ring, (5) 7x7x3mm bearings, (6) anular gear, (7) pinion and (8) front plate.

The main body of the robot is provided with a 1 DoF rotation mechanism about its longitudinal axis. In fact, the outer ring is the interface with the serial arm. It is designed to allow the main body to rotate freely by 360°, since it accommodates 18 bearings to allow for smooth rotation of the main body. Six of the 7x7x3mm bearings are distributed around the main body ring circumference, while the remaining 12 are split between front and back side of the ring, contained in the interface and its back plate (Fig. 3). In this way, rotation about the axis is facilitated by the peripheral bearings, while axial translation is constrained by the ones placed at the front and at the back of the main body's ring. Motion is transferred from the brushless motor to the main body through a pinion-annular gear coupling. The pinion has a reference diameter of 14mm and module 0.5. The annular gear is directly implemented in the interface with the serial arm through 3D printing, thus minimizing the amount of assembly work needed. The annular gear has a reference diameter of 56mm and module 0.5, therefore the gear reduction ratio is 1/4. The main body has a maximum diameter of 88mm and overall length of 240mm.

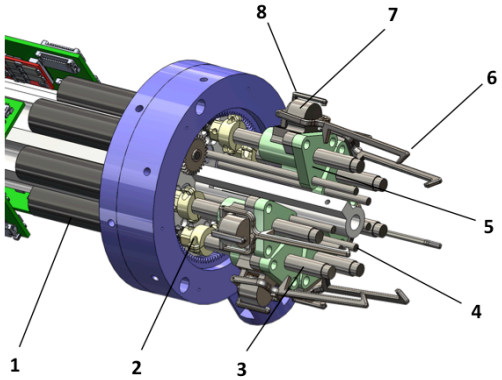

Figure 4. Detailed view of the linear actuators: (1) motors, (2) motor couplings, (3) 6mm leadscrews, (4) stability rods, (5) lead screw nuts, (6) slider hook, (7) load cell holders and (8) load cell pressing element.

The actuation of the end-effector, as mentioned above, relies on the use of six motors that drive as many 6 mm lead screws, with 1 mm lead and 59 mm long. The lead screws are connected to the motors through the use of flexible couplings to compensate for possible shafts misalignment. Each lead screw carries a precision anti-backlash nut ActiveCAM™ that allows moving precisely with a very small drag torque. In addition, a PTFE film is used to coat the screws and reduce friction between screw and nut. Considering that the nuts are 22.8mm long and the screws are 59mm, the nuts have a linear Range Of Motion (ROM) of 36.2mm. This ROM was designed to be larger than needed to maintain a higher degree of compatibility with customized instruments. Six Ø3mm stainless steel rods are used to maintain the orientation of the nuts, preventing them from rotating with the screw. These rods are fixed between the robot main body's ring and the front plate. The friction between the two components is once more very limited, due to the combination of stainless steel rod and the nut, which is made of a hard and self-lubricated Acetal (Fig. 4). Each lead screw nut also carries one load cell holder. This is inserted into the cylindrical opening of the carrier, which also allows the sensor's lead cable to exit from the side of the cavity. The lead cables are then routed through the hollow front shaft of the robot body, to the back of the robot main body, where the driving electronics is allocated (Fig. 5). The load cells used in these instruments are Futek LLB130 – FSH02950, they have a cylindrical shape with Ø9.5mm and thickness 3.3mm. The maximum load measurable is 222N, which is sufficiently large for the tendons used in the surgical instrument.

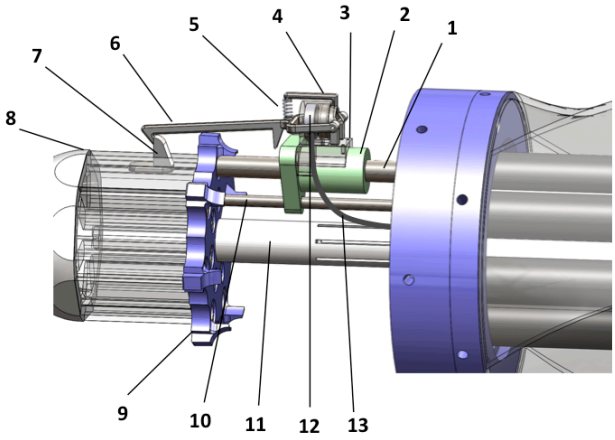

Figure 5. Detailed view of the slider nuts: (1) lead screw, (2) lead screw nut, (3) load cell holder, (4) load cell pressing element, (5) spring, (6) slider hook, (7) instrument's sliding coupling, (8) instrument proximal base, (9) front plate, (10) stability rod, (11) robot's front hollow shaft, (12) load cell and (13) load cell cable.

A pressing element is also inserted into the load cell holder and in contact with the load cell. This element is used to transmit the pulling force from the slider nut to the slider hook and therefore to the instrument. Doing this allows having a direct connection between the load cell and the instrument's tendons that are practically aligned at the instrument proximal end, thus simplifying the force measurement. The pressing element is provided with a hinge, where the slider hook can be attached. A spring with Internal Diameter (ID) of 2.3mm and Outside Diameter (OD) of 3mm and a rate of 77 N/mm is used to maintain the slider hooks engaged with the instrument's sliding couplings (Fig. 5). The robot front plate implements some cam-features for the automatic instrument release, when the slider nuts advance to their furthest position (Fig. 6). The slider hook also presents a contact element that uses the cam-feature to apply a load to the hook, which will culminate in a torque that will lift the hook from the instrument's sliding couplings, automatically releasing the surgical instrument.

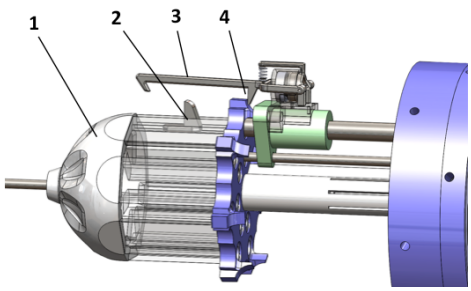

Figure 6. Detailed view of instrument release mechanism: (1) instrument proximal base, (2) sliding coupling, (3) slider hook and (4) cam featrure.

All the robot's components except from the motors, lead screws, nuts and bearings, are produced with rapid manufacturing techniques. The plastic components are made of a photopolymer cured with UV light and with similar mechanical properties to ABS. The metal components have been produced with Selective Laser Melting (SLM) of stainless steel 316.

C. *Instrument Design*

The robotic wristed instrument was designed to privilege the simplicity in the design. One of the drawbacks of additive manufacturing, especially when dealing with metal SLM, is that often components need a certain degree of post processing, for instance, to remove the support structure. In order to reduce the effect that this has on the full exploitation of rapid prototyping advantages, the tool was designed with the objective to reduce the overall number of components and simplify the assembly procedure. Generally speaking, the unit cost of additive manufacturing is higher than the one obtained with mass production in industrial processes. However, it is a cost-effective way of manufacturing at low volume and can achieve functionality and complexity that traditional manufacturing process cannot achieve. The instrument proposed in this work is realized of only 14 components, excluding the driving tendons. The assembly, with this degree of simplicity, only requires about 20minutes per instrument. Therefore, simplifying the assembly also contributes to reducing the unit cost, by reducing the labour needed to complete the assembly task (Fig. 7). In addition, having a limited unit cost allows to making the surgical tool disposable, further reducing the complexity of the design and manufacture, since there is no need to implement solutions for re-sterilization.

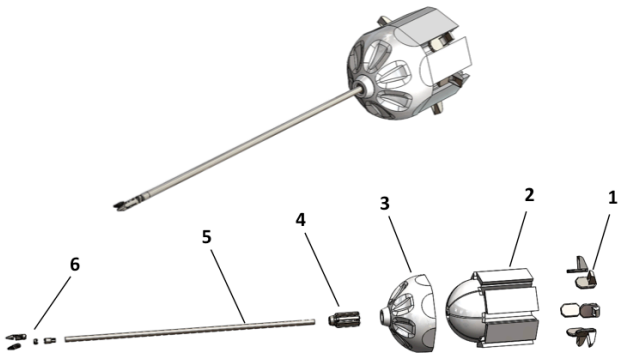

Figure 7. *Top:* wristed surgical grasper. *Bottom:* exploded view of the instrument. (1) sliding couplings, (2) proximal tool base, (3) base cover, (4) tendons separator, (5) rigid shaft and (6) wristed grasper.

The instrument proximal base and base cover are produced with rapid prototyping, using a Fused Deposition Modeling (FDM) printer with ABS as the material used. The instrument shaft is a stainless steel tube with OD3mm and ID2.5mm. The grasper components, the tendons separator and the sliding couplings are manufactured with SLM of stainless steel 316. The instrument's sliding couplings are actuated by the robot's slider hooks, which engage on the instruments couplings, after the tool is inserted and the slider hooks are moved backwards.

Stainless steel tendons are inserted in the sliding couplings and crimped to prevent tendons from escaping. The tendons chosen for this instruments have Ø0.35mm and strand 7x7. The breaking load of these tendons is about 80N, which is sufficient for the application devised for this instrument. The six tendons run from the sliding couplings towards the 3DoF end-effector, to actuate it as 3 pairs of antagonistic tendons. These last ones pass through a grove that is obtained on the dome shaped distal part of the instrument's base and in the internal part of its cover. The grove acts as a guide keeping the tendons path constant and providing a relatively low friction plastic-metal interface for the tendons. Successively, the six tendons enter the tendon separator at their respective place and are then routed together towards the instrument's end effector, passing through the rigid hollow shaft. The tendon separator is not provided of pulleys, which simplifies the construction. Although this design results in the tendons rubbing against the metal structure of the separator, the instrument performance for the intended use is not affected considering that the instruments is disposable and the friction deterioration effect is limited.

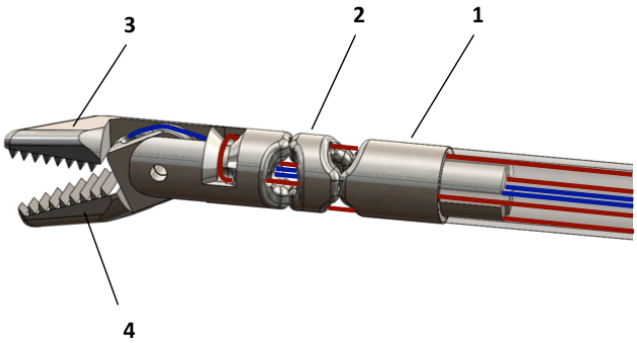

Figure 8. Detailed view of the instrument tip, (1) wrist base, (2) wrist link, (3) grasper fix link and (4) moving jaw. The tendons controlling the wrist are routed back on the grasper fix link (red) and the jaw ones are routed back and stamped inside the jaw tendon hole (blue).

The range of motion of the wrist is ±60° in both perpendicular planes and the grasper's motion can reach up to 90°, so it can behave as a grasper and as a dissector. The pair of tendons that actuates the grasper's jaw passes through the central hole of the wrist components, in order to reduce the coupling effect. One of the advantages of this design is that it is possible to redesign the instrument's tip and functionality and easily integrate it to the robot, by keeping the same instrument-robot coupling interface.

In fact, the main challenge of this design approach, when defining a new manufacturing protocol, is to finely tune and calibrate all the production variables until the method is well established for large and repeatable production. The goal is to find the right compromise between performance, durability and cost. For instance, the choice of materials represents an important step since prototyping materials might not have stable properties over time or might not match certain requirements, such as biocompatibility. Thus, a possible approach to produce this robot could be to produce with traditional manufacturing the main body of the robot and its components, while rapidly manufacturing only the disposable

instruments, therefore preserving also the possibility to customize the design of the instrument. The unitary production cost is estimated to be about £25, including the cost of rapidly manufacture metal and plastic components, the cost of purchasing the hollow tube and tendons and finally the assembly cost and time which is about 20min. Cost-effectiveness is proven by the fact that a traditional non-articulated laparoscopic instrument has a minimum selling price about £50.

III. Experiments

The experiments designed for this work aim to validate the capability of the robot to measure the interaction forces between the robotic instrument and the environment. The CY8CKIT-050 development board from Cypress Semiconductor is used to acquire data from the six load cells installed on the robot. On the board, a PSoC5LP (Programmable System-on-Chip) implements signal conditioning, amplification, and digitization. The data is sent to the host computer via USB communication. The set-up of these experiments includes the robot with its wristed surgical instrument and load cells. An additional external force gauge was used for the sole purpose of calibration and validation (Sauter FK250). This last one was grounded and fixed with respect to the instrument's rigid shaft, to avoid bias in the force reading at the tip of the instrument, due to possible rigid shaft deformations (Fig. 9).

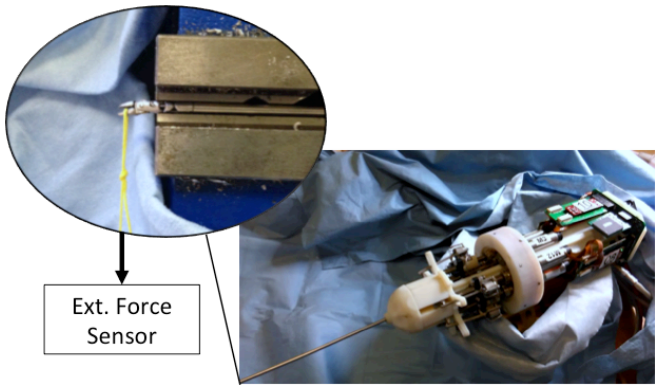

Figure 9. Experimental set-up: the grasper base is grounded together with the external force gauge to avoid bias in the measurement.

A. Calibration and Static Force Sensing

The first experiment was performed to characterize the relation between the load cell readings and the forces applied at the tip of the instrument. Each joint was tested individually for both antagonistic tendons. A spectra tendon with Ø0.46mm and breaking load of about 550N was used to connect the studied links to the external force sensor in the straightest configuration possible. Once the tool was positioned, tendons were preloaded at 2N to maintain certain stiffness in the instrument's tip. At this stage, the tested joint was actuated to pull the link away from the external force sensor and therefore apply a torque to it. The test was arrested before reaching too high values of tendon tension that could damage the instrument.

The four tendons needed to actuate the wrist pass at a distance of about 0.5mm from the respective joint's rotation axis. This is a very short leverage that on the other hand acts as tension amplifier when reading the tendons' tension measured by the load cells. In fact, for smaller leverage, the force required to actuate the joint is higher; therefore the force reading on the tendon will be increased as the lateral load at the tip of the instruments has a larger cantilever than the cantilever of the tendon. The load cantilever for Joint 1 was measured as 10.3mm, while for Joint 2 it was 8mm. With respect to the grasper test, the load was applied at an approximate distance of 8mm from the pivot axis of the grasper's jaw, while the actuation tendon had a cantilever of about 0.8mm with respect to the jaw pivot axis (Fig. 10).

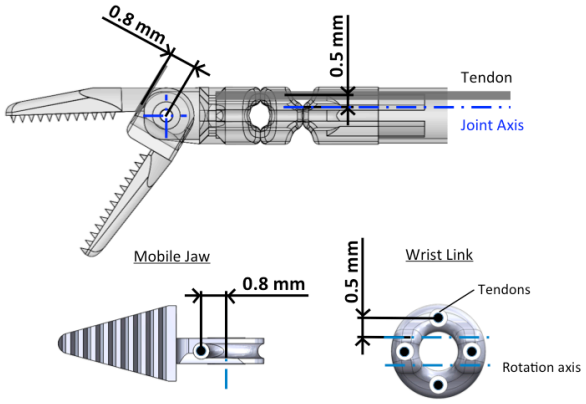

Figure 10. Representation of the tendons cantilevers with respect to the rotation axis of the jaw and the wrist link.

Figure 11 shows the relation between the force required to pull the tendons and the force applied by the instrument's tip to the external force sensor. The response of the sensing system, as visible from the graphs, is quite linear for all the three joints. Furthermore, because the response of pairs of antagonistic tendons was very similar, the results of antagonistic pairs were averaged. The analogue signal coming from the load cells was amplified and filtered with a low-pass filter with cut-off frequency of 10Hz. Consequently, the final residual noise was measured to be about ±0.5N and therefore was negligible for the results. The variations of the measured load with respect to the ideal straight line are due to structural deformation of some elements of the system and also friction. Increasing tendon tensions leads to higher friction between the sliders and their rails. As visible from the graphs related to Joint 1 and Joint 2, the load cell on the tendons of Joint 2 is capable of measuring more lateral force at the tip than in the case of Joint 1. This is due to the fact that, the lateral force on Joint 1 has a larger cantilever with respect to Joint 2. This will cause the tension of the tendons of the first joint to be higher.

B. *Object Grasping with Force Sensing*

After calibrating and validating the force measurement, an experiment was designed to test force sensing while actuating the instrument and grasping an object. This was used to validate the functionality of the robot. An automated routine was also developed to automatically pretension all the tendons at 2N and then hold the position.

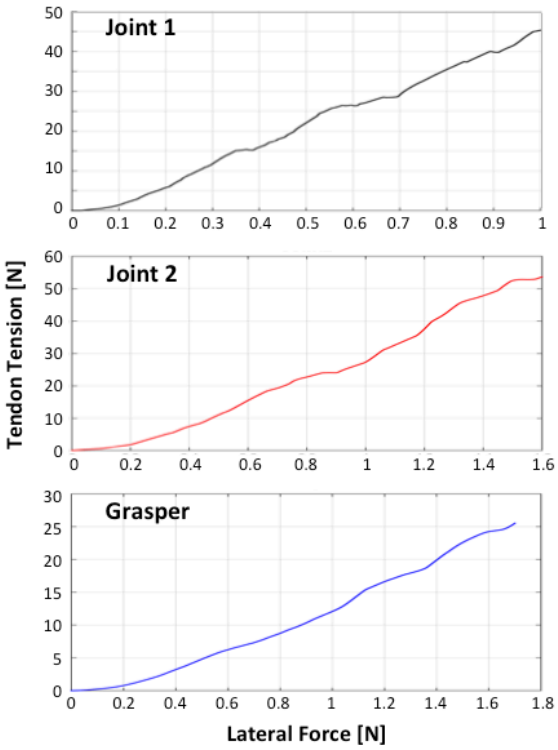

Figure 11. Experimental results for the experiment 1, the load cells can measure the force applied at the tip with a linear response. Data were filtered with a low-pass-filter and the behaviour of the antagonistic tendons was averaged because very similar. Joint 1 is the most proximal to the tool base, followed by Joint 2 and the Grasper.

A simple control scheme was devised to control the antagonistic pair of tendons independently with two motors. In order to easily measure the force applied to the end-effector and propagated to its driving tendon, the control had to be decoupled between the two tendons. Therefore, one motor was controlled using a traditional PID loop with position and velocity as set points, while the control for the second motor included the same PID loop with an additional external loop with the objective of maintaining the pretension on the tendon (Fig. 12).

Xs1 and Vs1 are respectively the position and velocity set points for Motor 1 (M1). These variables are used as an input to control the position of the robotic instrument by the user. The tension on the first tendon is measured by the load cell and converted into the load applied at the tip of the instrument. This is easily done by subtracting the tension of the second tendon from the first one and therefore by scaling by the correct amount found with the first experiment. The second control loop is using the pretension value as input; as a result the motor tries to hold the tension on the second tendon at the pre-set value of 2N. Therefore, the tension readings from the two branches result to be decoupled and measuring the lateral load at the tip while controlling the instrument in the space is possible.

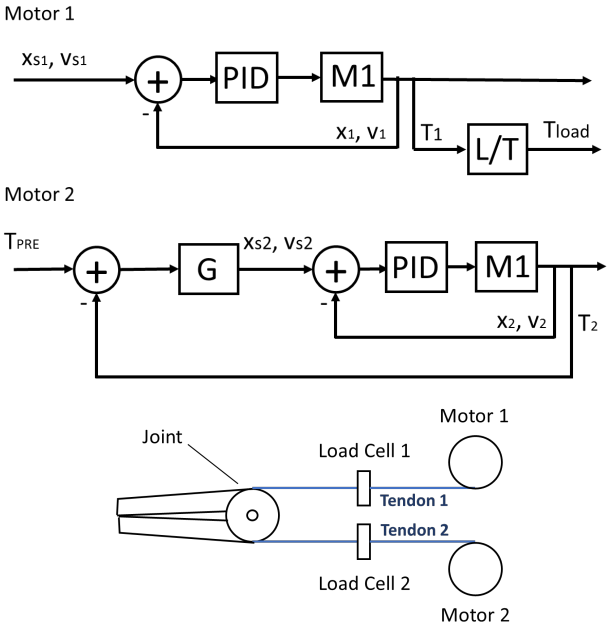

Figure 12. *Above:* Control scheme of one joint of the insturment. Two loops are used to control the two antagonistic tendons. One motor controls the position, while the second one controls the tensioning. *Below:* semplified scheme of the tendon management for one joint.

Figure 13 shows the results from the second experiment. In this experiment the grasper moving jaw was used to pull the spectra tendon connected to the external force sensor, while the second motor was compensated for the tension, trying to keep it constant to the preload value. The initial conditions of this experiment were the same as after the automated tensioning routine, therefore the tension on both tendons was equal to 2 N. The grasper's jaw was connected to the spectra cable, which was the object to grasp, that was tied to the external load sensor. This last one confirmed once more that the transformation between force at the tip and tendon tension was quite linear, therefore was omitted from the graph.

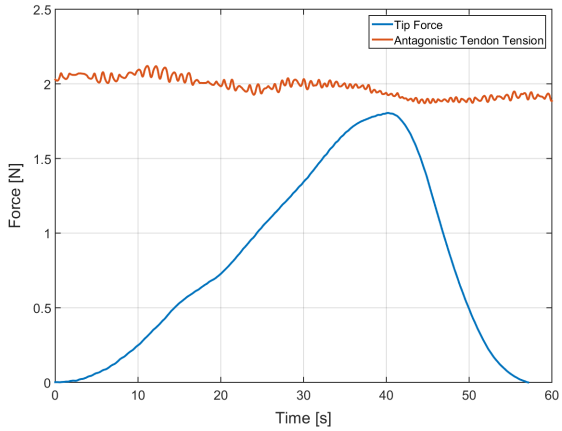

Figure 13. Force measured during grasping. The blue line represents the interaction force between grasper and the object measured with the robot, while the red line shows the tendon tension applied to the second tendon and kept constant by the motor.

From Figure 13, it can be seen that the grasping task was 1 minute long and the force measuring on the first tendon showed comparable results to the first experiment. At about 40s the pulling force of the jaw started to be reduced to prevent the tendons from being damaged. The tension on the first tendon is basically the same as the blue line, but scaled up to the tendon tension values. Furthermore, the red line represents the tension on the second tendon; this one clearly fluctuates about 2N, which is the pre-set tensioning and also the set point of the control loops of Motor 2. The controller was using a stability threshold of 0.5N on the tendon tension to prevent the second motor from continuously change direction, due to the residual noise. This helped to stabilize the control, although some tension oscillations were still present on the second tendon. As observable at 40s, when the grasper's pulling force starts to decrease, there is also a slight drop on the second tendon's tension. This is due to the fact of how the controller was designed. When changing direction, Motor 1 is not pulling but releasing the tendon; therefore the load cell on the second tendon measures a drop in tension and actuates Motor 2 in the opposite direction with respect to the previous situation.

Finally, an experiment to evaluate the repeatability of the position control was carried out. The instrument's tip was moved in the space while actuating the most proximal joint in a cyclic way across the whole ROM. The wrist joint chosen was the one further away from the instrument's tip, since a larger distance introduces higher uncertainty. To track the instrument's tip, an electro-magnetic marker was mounted on the instrument's fixed jaw and tracked with the system *trakSTAR* (by NDI). It resulted that the deviation in positioning was varying between 1.5 and 3mm (Fig. 13), according to where the joint was in the space. In addition to it, the instrument broke after the completion of about 850 motion cycles. Both repeatability and durability tests show promising results for the deployment of rapidly manufactured-disposable instruments in the clinical practice.

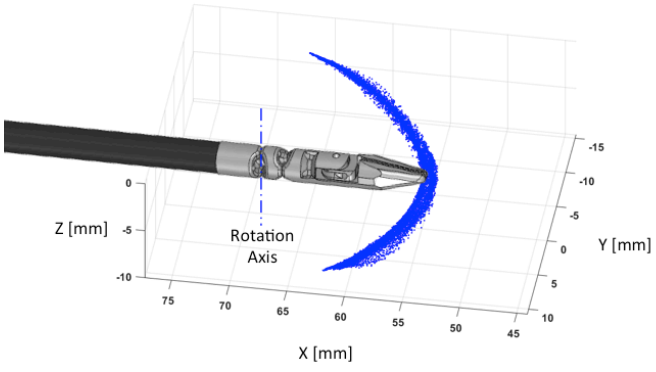

Figure 14. Position control repeatability, while actuating the first wrist joint. The repeatability varies between 1.5mm and 3mm.

IV. Conclusion

This work proposed the design of a surgical robot that uses smart concepts to fully exploit the advantages of 3D printing, modularity and force sensing. The robot gives the possibility of connecting customizable instruments to a quick automated coupling. In addition, the robot is capable of fully monitoring the force exchanged with the instrument's couplings and therefore to reconstruct the forces applied by the instrument. In a similar way, the same force sensing capabilities can be used to increase safety and detect possible damage to the instrument. Two sets of experiments were conducted to validate the force sensing capabilities of the robot and calibrate the system. The force measurement resulted to be quite linear, although some residual noise is still present. With regards to the clinical translation process, preliminary repeatability and durability tests have shown promising results that suggest the disposable instruments could be deployed in a real surgical scenario, after some minor improvements. Dedicated work should aim to finalize completely the manufacturing protocol and life cycle of an instrument to obtain the necessary certifications. In the meantime, future work will aim to improve the control algorithm, in order to achieve a more stable control for tension compensation.

References

[1] Yasa, E., & Kruth, J. P. (2011). Microstructural investigation of Selective Laser Melting 316L stainless steel parts exposed to laser remelting. Procedia Engineering, 19, 389-395.

[2] Ahn, S. H., Lee, K. T., Kim, H. J., Wu, R., Kim, J. S., & Song, S. H. (2012). Smart soft composite: an integrated 3D soft morphing structure using bend-twist coupling of anisotropic materials. *International Journal of Precision Engineering and Manufacturing*, *13*(4), 631-634.

[3] Azari, A., & Nikzad, S. (2009). The evolution of rapid prototyping in dentistry: a review. *Rapid Prototyping Journal*, *15*(3), 216-225.

[4] Wu, G., Zhou, B., Bi, Y., & Zhao, Y. (2008). Selective laser sintering technology for customized fabrication of facial prostheses. *The Journal of prosthetic dentistry*, *100*(1), 56-60.

[5] Petzold, R., Zeilhofer, H. F., & Kalender, W. A. (1999). Rapid prototyping technology in medicine—basics and applications. *Computerized Medical Imaging and Graphics*, *23*(5), 277-284.

[6] Traeger, M. F., Roppenecker, D. B., Leininger, M. R., Schnoes, F., & Lueth, T. C. (2014, September). Design of a spine-inspired kinematic for the guidance of flexible instruments in minimally invasive surgery. In *Intelligent Robots and Systems (IROS 2014), 2014 IEEE/RSJ International Conference on* (pp. 1322-1327). IEEE.

[7] Gosline, A. H., Vasilyev, N. V., Veeramani, A., Wu, M., Schmitz, G., Chen, R., ... & Dupont, P. E. (2012, May). Metal MEMS tools for beating-heart tissue removal. In *Robotics and Automation (ICRA), 2012 IEEE International Conference on* (pp. 1921-1926). IEEE.

[8] Seneci, C. A., Shang, J., Darzi, A., & Yang, G. Z. (2015, September). Rapid manufacturing with selective laser melting for robotic surgical tools: Design and process considerations. In *Intelligent Robots and Systems (IROS), 2015 IEEE/RSJ International Conference on* (pp. 824-830). IEEE.